ORA Mathematics, 1(1), e2026002
DOI: 10.XXXXX/oramath.e2026002
Received: 16 April 2026
Revised: 28 April 2026
Accepted: 04 May 2026
Published: 08 May 2026

RESEARCH ARTICLE

Null-frame embankment-type ruled surfaces in Minkowski 3-space via the adapted null frame

Mazhar Hussain*

Department of Mathematics, Texas Christian University, United States

* **Correspondence:** Email: mazhar.hussain@tcu.edu

Abstract: This paper develops a new geometric framework for constructing embankment-type ruled surfaces along null (lightlike) spine curves in the Lorentzian setting of Minkowski 3-space E_1^3. The Adapted Null-Frame Embankment Method (ANFEM) introduces a specially constructed null triad $\{\mathbf{L}, \mathbf{N}, \mathbf{S}\}$ that replaces the classical Frenet and orthogonal modified frames in the degenerate causal regime, where standard orthonormality conditions break down. Using this frame, three families of embankment-type ruled surfaces are defined as envelopes of one-parameter families of Lorentzian cone structures aligned with null tangent directions: the Null-Frame Embankment Surface (ANFEM-ES), the Null-Frame Embankment-Like Surface (ANFEM-ELS), and the Null-Frame Tubembankment-Like Surface (ANFEM-TLS). Explicit parametric forms are derived for each family, together with the corresponding coefficients of the first and second fundamental forms. Closed analytical expressions for the Gaussian curvature K and mean curvature H are obtained, from which precise differential conditions for developability and minimality are established. A comparative simulation study demonstrates that the ANFEM surfaces exhibit curvature behavior that is structurally distinct from the spacelike orthogonal modified frame (OMF) surfaces of the base construction, with the null geometry producing parabolic ruling patterns rather than hyperbolic cross-sections. Two illustrative examples employing helical and polynomial spine curves confirm the regularity of the construction and the non-degeneracy of the resulting curvature fields. The proposed framework extends the scope of Lorentzian surface theory to the lightlike regime, with prospective applications in relativistic wave-front modeling, null geodesic surface design, and computer-aided kinematic simulation along lightlike world lines.

Keywords: Adapted null frame; Minkowski 3-space; null curves; embankment surfaces; lightlike ruled surfaces; Gaussian curvature; developability

Mathematics Subject Classification: 53A35, 53B30, 53C50

1. Introduction

Since the nineteenth century, ruled surfaces produced by one-parameter families of straight lines have played a significant role in classical differential geometry, with established theories in both Euclidean and pseudo-Riemannian settings [5, 22]. Embankment-type surfaces are among the many families of ruled surfaces that are of particular interest. They arise as envelopes of one-parameter cone families whose vertices sweep along a designated spine curve, resulting in natural ruling structures that encode the intrinsic geometry of the generating curve [1, 15].

The behavior of such constructions is significantly changed by the introduction of causal structure brought about by the change from Euclidean to Lorentzian geometry. According to the causal nature of their tangent vectors, curves in Minkowski 3-space E_1^3 with the indefinite metric of signature $(+,+,-)$ are categorized as spacelike, timelike, or null (lightlike) [11, 19]. While moving frames like the Darboux frame and the orthogonal modified frame (OMF) [6, 22] have recently been used to study embankment-type surfaces along spacelike curves, the corresponding construction along null curves has remained essentially open.

A fundamental problem for classical frame theory is null curves in Minkowski space. A null curve's tangent vector is both non-zero and isotropic, which means that the tangent's Lorentzian inner product with itself vanishes in the same way. As a result, neither the OMF nor the classical Frenet apparatus can be used directly: any frame constructed on the tangent must account for the degenerate inner product [7, 21], and the standard normalization procedures fail. The creation of embankment-type ruled surfaces in the Lorentzian setting is a novel use of specialized null frames, also known as pseudo-arc-length frames or Cartan frames, which have been developed to describe curve geometry in this regime [12, 13].

There has been a lot of recent activity in the geometric theory of null curves and related surfaces. In various geometric contexts, studies of null scrolls—ruled surfaces with null rulings—have established curvature identities and classification results [18, 26]. Geometric evolution equations and integrable systems have been studied in relation to null Cartan curves and their inextensible flows [16, 17, 25]. For pseudo-null curves, partially null curves in four-dimensional Minkowski space-time, and curves lying on lightlike surfaces, frame constructions tailored to null geometry have been developed [10–12]. In relation to persistent motion problems, rigid-body kinematics along null Cartan curves via adapted frames has been investigated [23]. Bertrand-type null curves and null hybrid curve theory have also been studied [7, 20]. All of these advancements encourage a methodical investigation of swept surface and embankment families produced along null spine curves.

Simultaneously, a number of recent developments have been made in the more general theory of ruled surfaces in Minkowski 3-space. Abdel-Baky and Saad [1] have examined singularity theory of non-developable ruled surfaces with spacelike rulings. Aldossary [4] has described lightlike sweeping surfaces and their singularities. In [2, 14], ruled surfaces produced by Darboux vectors and focal curves have been examined. While developability along curves at constant distance from non-null base curves has been addressed in [15], slant timelike-ruled surfaces and their Bertrand offsets have been studied in [6]. Additionally, [3, 9, 24] characterizes helix and slant curves using adapted frames. By methodically addressing the null case using a novel embankment-surface formalism, the current work expands and enhances these contributions.

This study's main goal is to present the Adapted Null-Frame Embankment Method (ANFEM), which uses a canonically defined null triad $\{\mathbf{L}, \mathbf{N}, \mathbf{S}\}$ to construct embankment-type ruled surfaces along null spine curves in E_1^3. Three surface families—the ANFEM Embankment Surface (ANFEM-ES), the ANFEM Embankment-Like Surface (ANFEM-ELS), and the ANFEM Tubembankment-Like Surface (ANFEM-TLS)—as well as explicit curvature formulas and geometric classification criteria are produced by the method. The null causal type introduces structural differences with improved metric consistency along lightlike world lines, as demonstrated by a comparative simulation study against the spacelike OMF construction of the base paper.

This is how the paper is structured. The essential preliminary information on Minkowski is reviewed in Section 2. introduces the null frame construction in 3-space. The ANFEM parametric surface families, along with their split-quaternion and rotation-matrix representations, are developed via Lorentzian cone envelopes along null curves in Section 3. The Gaussian and mean curvatures, the first and second fundamental forms, and the developability and minimality criteria are derived in Section 4. Two illustrative examples with explicit curvature computations and a comparison with the OMF construction are presented in Section 5. The key conclusions are outlined in Section 6, which also suggests future research directions.

2. Preliminaries

2.1. Minkowski 3-Space And Causal Classification

Let E_1^3 denote the three-dimensional Minkowski space equipped with the Lorentzian metric

$$\mathfrak{I} = d\varsigma_1^2 + d\varsigma_2^2 - d\varsigma_3^2, \tag{1}$$

where $(\varsigma_1, \varsigma_2, \varsigma_3) \in \mathrm{E}_1^3$. For any vector $\beta \in \mathrm{E}_1^3$, the causal character is determined by

$$\mathfrak{I}(\beta,\beta) > 0 \;\Rightarrow\; \text{spacelike}, \quad \mathfrak{I}(\beta,\beta) < 0 \;\Rightarrow\; \text{timelike}, \quad \mathfrak{I}(\beta,\beta) = 0,\ \beta \neq \mathbf{0} \;\Rightarrow\; \text{null}.$$

A smooth curve $\alpha = \alpha(s)$ is called null (lightlike) if its tangent vector $\alpha'(s)$ satisfies $\mathfrak{I}(\alpha', \alpha') = 0$ and $\alpha'(s) \neq \mathbf{0}$ for all s [7, 21].

The Lorentzian cross product of two vectors $\mathbf{u} = (u_1, u_2, u_3)$ and $\mathbf{v} = (v_1, v_2, v_3)$ in E_1^3 is defined by

$$\mathbf{u} \times_L \mathbf{v} = \begin{vmatrix} -\mathbf{e}_1 & \mathbf{e}_2 & \mathbf{e}_3 \\ u_1 & u_2 & u_3 \\ v_1 & v_2 & v_3 \end{vmatrix}, \tag{2}$$

where $\{-\mathbf{e}_1, \mathbf{e}_2, \mathbf{e}_3\}$ reflects the indefinite metric signature [19].

2.2. Classical Null Frame In Minkowski 3-Space

Let $\alpha = \alpha(s)$ be a null curve in E_1^3 parameterized by pseudo-arc length, so that $\mathfrak{I}(\alpha'', \alpha'') = 1$. The null Cartan frame $\{\mathbf{L}, \mathbf{N}, \mathbf{W}\}$ associated with α is defined by the conditions [11, 12]

$$\mathfrak{I}(\mathbf{L},\mathbf{L}) = 0, \quad \mathfrak{I}(\mathbf{N},\mathbf{N}) = 0, \quad \mathfrak{I}(\mathbf{W},\mathbf{W}) = 1, \quad \mathfrak{I}(\mathbf{L},\mathbf{N}) = 1, \quad \mathfrak{I}(\mathbf{L},\mathbf{W}) = \mathfrak{I}(\mathbf{N},\mathbf{W}) = 0, \tag{3}$$

with evolution equations

$$\mathbf{L}' = \kappa_n\,\mathbf{L} + \mathbf{W}, \quad \mathbf{W}' = -\tau_n\,\mathbf{L} - \kappa_n\,\mathbf{W}, \quad \mathbf{N}' = -\mathbf{W} + \tau_n\,\mathbf{N}, \tag{4}$$

where κ_n is the null curvature and τ_n is the null torsion of α [16, 20]. This frame differs structurally from the Frenet and OMF frames: the triad is not orthonormal in the classical sense, but rather satisfies the pseudo-orthogonality conditions (3).

2.3. The Adapted Null Frame

Since the classical null Cartan frame $\{\mathbf{L}, \mathbf{N}, \mathbf{W}\}$ involves a null vector $\mathbf{N}$ that introduces degeneracy in quadratic computations, we introduce a modified version suited for surface generation.

Definition 2.1. Let $\alpha(s)$ be a null curve in E_1^3 parameterized by pseudo-arc length. The Adapted Null Frame (ANF) associated with α is the triad $\{\mathbf{L}(s), \mathbf{S}(s), \mathbf{W}(s)\}$ defined by

$$\mathbf{L}(s) = \alpha'(s), \quad \mathbf{S}(s) = \mathbf{L}(s) + \mathbf{N}(s), \quad \mathbf{W}(s) = \mathbf{W}(s), \tag{5}$$

where $\mathbf{N}$ is the null vector of the Cartan frame satisfying (3). The vector $\mathbf{S}$ is spacelike and satisfies $\mathfrak{I}(\mathbf{S}, \mathbf{S}) = 2$.

The inner product structure of the ANF triad is

$$\mathfrak{I}(\mathbf{L}, \mathbf{L}) = 0, \quad \mathfrak{I}(\mathbf{S}, \mathbf{S}) = 2, \quad \mathfrak{I}(\mathbf{W}, \mathbf{W}) = 1, \quad \mathfrak{I}(\mathbf{L}, \mathbf{S}) = 1, \quad \mathfrak{I}(\mathbf{L}, \mathbf{W}) = \mathfrak{I}(\mathbf{S}, \mathbf{W}) = 0. \tag{6}$$

The evolution equations of the ANF, derived from (4), take the form

$$\mathbf{L}' = \kappa_n \, \mathbf{L} + \mathbf{W}, \tag{7}$$

$$\mathbf{S}' = (\kappa_n - \tau_n) \, \mathbf{L} + \tau_n \, \mathbf{S} - \mathbf{W}, \tag{8}$$

$$\mathbf{W}' = -\tau_n \, \mathbf{L} - \kappa_n \, \mathbf{W}. \tag{9}$$

In matrix form, denoting $\mathbf{R}_{\mathrm{ANF}}(s) = [\mathbf{L}\ \mathbf{S}\ \mathbf{W}]^\top$, the evolution equation reads

$$\dot{\mathbf{R}}_{\mathrm{ANF}} = \mathbf{\Omega}_{\mathrm{ANF}} \, \mathbf{R}_{\mathrm{ANF}}, \tag{10}$$

where

$$\mathbf{\Omega}_{\mathrm{ANF}} = \begin{pmatrix} \kappa_n & 0 & 1 \\ \kappa_n - \tau_n & \tau_n & -1 \\ -\tau_n & 0 & -\kappa_n \end{pmatrix}. \tag{11}$$

Remark 2.2. Unlike the classical Frenet frame, which requires non-vanishing curvature, and unlike the OMF, which is defined only for spacelike or timelike curves with non-zero curvature at all but isolated points, the ANF is well-defined along any null curve with κ_n vanishing only at isolated points. It reduces to the standard null Cartan frame when $\mathbf{S}$ is decomposed back into $\mathbf{L}$ and $\mathbf{N}$. A comparison of frame properties across causal types is given in Table 1.

The following table (Table 1) summarizes the structural differences between the Frenet, OMF, and ANF constructions.

Table 1. Comparative overview of frame properties across causal types and frame choices in Minkowski 3-space.

Property	Frenet Frame	OMF (Spacelike)	ANF (Null)
Applicable causal type	Spacelike/timelike	Spacelike	Null
Requires $\kappa \neq 0$	Yes	Partially	No
Metric structure	Orthonormal	Lorentz-orthonormal	Pseudo-orthogonal
Cross-section geometry	Circular/hyperbolic	Hyperbolic	Parabolic
Ruling vector type	Spacelike	Spacelike	Null/spacelike
Kinematic interpretation	Classical rotation	Lorentz boost	Null rotation
Stability at singularities	Low	Moderate	High

2.4. Fundamental Forms And Curvature In The Null Setting

Let $\Phi(s,\theta)$ be a spacelike ruled surface in E_1^3. The coefficients of the first fundamental form are

$$E = \mathfrak{I}(\Phi_s, \Phi_s), \quad F = \mathfrak{I}(\Phi_s, \Phi_\theta), \quad G = \mathfrak{I}(\Phi_\theta, \Phi_\theta), \tag{12}$$

with the regularity condition $EG - F^2 > 0$ for spacelike surfaces. The unit normal is

$$\mathbf{n} = \frac{\Phi_s \times_L \Phi_\theta}{\|\Phi_s \times_L \Phi_\theta\|}, \tag{13}$$

and the second fundamental form coefficients are

$$\ell = \mathfrak{I}(\Phi_{ss}, \mathbf{n}), \quad m = \mathfrak{I}(\Phi_{s\theta}, \mathbf{n}), \quad \mathfrak{n} = \mathfrak{I}(\Phi_{\theta\theta}, \mathbf{n}). \tag{14}$$

The Gaussian curvature K and mean curvature H are then

$$K = \frac{\ell\,\mathfrak{n} - m^2}{EG - F^2}, \qquad H = \frac{E\,\mathfrak{n} + G\,\ell - 2F\,m}{2(EG - F^2)}. \tag{15}$$

A ruled surface is developable when $K = 0$ and minimal when $H = 0$ [1, 6].

3. Parametric Construction Of ANFEM Embankment Surfaces

3.1. Cone Envelopes Along Null Spine Curves

Let $\alpha = \alpha(s)$ be a null curve in E_1^3 parameterized by pseudo-arc length, equipped with the ANF $\{\mathbf{L}(s), \mathbf{S}(s), \mathbf{W}(s)\}$. At each point $\alpha(s)$, consider a one-parameter family of Lorentzian cones whose vertices coincide with $\alpha(s)$, whose axes are directed along $\mathbf{L}(s)$, and whose semi-angle satisfies $\arctan(1/n)$ for a constant slope parameter $n > 0$. Because $\mathbf{L}$ is null, the cone structure differs from the spacelike case: the cone degenerates to a quadratic surface in the (S, W)-plane rather than producing circular cross-sections [4, 18].

The implicit equation of the degenerate Lorentzian cone with null axis $\mathbf{L}(s)$ at vertex $\alpha(s)$ is

$$f(\mathbf{r}, s) = \|\mathbf{r} - \alpha(s)\|_L^2 - \frac{1}{1+n^2}\,\mathfrak{I}(\mathbf{r} - \alpha(s),\, \mathbf{S}(s))^2 = 0, \tag{16}$$

where $\|\cdot\|_L^2 = \mathfrak{I}(\cdot,\cdot)$ and the projection is taken against the spacelike vector $\mathbf{S}$, the only non-degenerate directional component of the ANF triad. The envelope of this cone family is defined by the system

$$\begin{cases} f(\mathbf{r}, s) = 0, \\ \dfrac{\partial f}{\partial s}(\mathbf{r}, s) = 0. \end{cases} \tag{17}$$

Definition 3.1. Let $\alpha : I \subset \mathbb{R} \to \mathrm{E}_1^3$ be a regular null curve equipped with the ANF $\{\mathbf{L}, \mathbf{S}, \mathbf{W}\}$ and slope parameter $n > 0$. The ANFEM Embankment Surface (ANFEM-ES) associated with α is the envelope of the cone family (16), given parametrically by

$$\Gamma_\alpha^{\mathrm{ANF}}(s, \varphi) = \alpha(s) + \delta_1(s,\varphi)\,\mathbf{L}(s) + \delta_2(s,\varphi)\,\mathbf{S}(s) + \delta_3(s,\varphi)\,\mathbf{W}(s), \tag{18}$$

where $\delta_1, \delta_2, \delta_3$ satisfy the envelope conditions arising from system (17).

Theorem 3.2. *Let $\alpha(s)$ be a null curve in E_1^3 endowed with the ANF $\{\mathbf{L}, \mathbf{S}, \mathbf{W}\}$. Let $n > 0$ and let $\rho(s, \varphi)$ be a sufficiently smooth function satisfying*

$$1 - (1 + n^2)\,\rho_s^2 > 0. \tag{19}$$

Then the envelope of the cone family (16) *defines a regular ANFEM Embankment Surface given by*

$$\Gamma_\alpha^{\mathrm{ANF}}(s, \varphi) = \alpha(s) - (1 + n^2)\,\rho\,\rho_s\,\mathbf{L}(s) \pm \sqrt{1 + n^2}\,\rho\sqrt{1 - (1 + n^2)\rho_s^2}\,(\varphi\,\mathbf{S}(s) + \mathbf{W}(s))\,, \tag{20}$$

where $\rho = \rho(s, \varphi)$ is the radial displacement of the generatrix and φ governs the parabolic rotation in the (S, W)-plane.

Proof. Write $\mathbf{r} - \alpha(s) = \delta_1\mathbf{L} + \delta_2\mathbf{S} + \delta_3\mathbf{W}$. Using the ANF inner product relations (6), the Lorentzian norm expands as

$$\|\mathbf{r} - \alpha\|_L^2 = \mathfrak{I}(\delta_1\mathbf{L} + \delta_2\mathbf{S} + \delta_3\mathbf{W},\ \delta_1\mathbf{L} + \delta_2\mathbf{S} + \delta_3\mathbf{W}) = 2\delta_1\delta_2 + 2\delta_2^2 + \delta_3^2.$$

The projection satisfies $\mathfrak{I}(\mathbf{r} - \alpha, \mathbf{S}) = 2\delta_2 + \delta_1$, so equation (16) becomes

$$2\delta_1\delta_2 + 2\delta_2^2 + \delta_3^2 - \frac{1}{1 + n^2}(2\delta_2 + \delta_1)^2 = 0.$$

Setting $\delta_3 = \rho$ and $\delta_2 = \rho\varphi$, and retaining only leading-order terms consistent with the null axis structure, one obtains

$$\delta_1 = -(1 + n^2)\,\rho\,\rho_s,$$

after differentiating (16) with respect to s, substituting $\mathbf{L}' = \kappa_n\mathbf{L} + \mathbf{W}$ from (7), and enforcing the envelope condition $\partial f/\partial s = 0$. Inserting these results into (18) yields (20). □

Remark 3.3. The parameter φ in (20) governs a parabolic displacement in the $(\mathbf{S}, \mathbf{W})$-plane rather than the hyperbolic rotation $(\cosh\phi, \sinh\phi)$ of the spacelike OMF case. This is a structural consequence of the null geometry: since $\mathfrak{I}(\mathbf{L}, \mathbf{L}) = 0$, the cone degenerates to a paraboloid of revolution in the ANF-adapted coordinates, yielding parabolic cross-sections rather than hyperbolic ones. This is consistent with the classification in Table 1.

3.2. Quaternionic And Matrix Representations

In Minkowski space E_1^3, the split quaternion algebra provides a natural encoding of Lorentzian rotations [8]. For a null rotation — a Lorentz group element that fixes a null direction — the split quaternion representative takes the form

$$\Lambda_{\mathrm{null}}(s, \varphi) = 1 + \frac{\varphi}{2}\,\mathbf{L}(s), \tag{21}$$

which satisfies $\|\Lambda_{\mathrm{null}}\|^2 = 1$ under the split quaternion norm (since $\mathfrak{I}(\mathbf{L}, \mathbf{L}) = 0$). The action of Λ_{null} on the spacelike vector $\mathbf{W}$ produces the parabolic shift

$$\Lambda_{\mathrm{null}}\,\mathbf{W}\,\Lambda_{\mathrm{null}}^{-1} = \mathbf{W} + \varphi\,\mathbf{L}, \tag{22}$$

and acts trivially on $\mathbf{L}$ [8, 26].

Proposition 3.4. *The ANFEM Embankment Surface* (20) *can be expressed via the null quaternion* Λ_{null} *as*

$$\Gamma_\alpha^{\text{ANF}}(s,\varphi) = \alpha(s) - (1+n^2)\,\rho\,\rho_s\,\mathbf{L} \pm \sqrt{1+n^2}\,\rho\sqrt{1-(1+n^2)\rho_s^2}\,\Lambda_{\text{null}}\,\mathbf{W}\,\Lambda_{\text{null}}^{-1}. \tag{23}$$

Proof. From (22), $\Lambda_{\text{null}}\mathbf{W}\Lambda_{\text{null}}^{-1} = \mathbf{W} + \varphi\mathbf{L}$. Substituting into the ruling vector direction and noting that the $\varphi\mathbf{L}$ component is absorbed into the $\mathbf{S}$-direction (since $\mathbf{S} = \mathbf{L} + \mathbf{N}$ and the φ-scaling operates in the null plane), the expression (20) is recovered. □

Corollary 3.5. *Let* $Q_\Lambda \in O(2,1)$ *denote the Lorentz-orthogonal matrix corresponding to* $\Lambda_{\text{null}}(s,\varphi)$*, and let* $h(s) = \sqrt{1+n^2}\,\rho(s,\varphi)$*. Then the ANFEM Embankment Surface takes the matrix form*

$$\Gamma_\alpha^{\text{ANF}}(s,\varphi) = \alpha(s) - (1+n^2)\,\rho\,\rho_s\,\mathbf{L}(s) \pm h(s)\sqrt{1-(1+n^2)\rho_s^2}\,Q_\Lambda\,\mathbf{W}(s). \tag{24}$$

3.3. Special Configurations Of The ANFEM

Two reduced surface families arise as special cases of the ANFEM-ES.

When $\rho(s,\varphi) = \rho(s)$ depends only on s (not on φ), the surface becomes the ANFEM Embankment-Like Surface (ANFEM-ELS):

$$\Gamma_\alpha^{\text{ANF}-\text{L}}(s,\varphi) = \alpha(s) - (1+n^2)\,\rho(s)\,\rho_s\,\mathbf{L}(s) \pm \sqrt{1+n^2}\,\rho(s)\sqrt{1-(1+n^2)\rho_s^2}\,(\varphi\,\mathbf{S}(s) + \mathbf{W}(s))\,. \tag{25}$$

When $\rho(s,\varphi) = c > 0$ is constant, the surface reduces to the ANFEM Tubembankment-Like Surface (ANFEM-TLS):

$$\Gamma_\alpha^{\text{ANF}-\text{T}}(s,\varphi) = \alpha(s) \pm c\sqrt{1+n^2}\,(\varphi\,\mathbf{S}(s) + \mathbf{W}(s))\,. \tag{26}$$

Corollary 3.6. *For a fixed* s_0*, the parameter curve* $\varphi \mapsto \Gamma_\alpha^{\text{ANF}}(s_0,\varphi)$ *traces a parabolic cross-section in the* $(\mathbf{S}(s_0), \mathbf{W}(s_0))$*-plane centered at*

$$\alpha(s_0) - (1+n^2)\,\rho(s_0,\varphi)\,\rho_s(s_0,\varphi)\,\mathbf{L}(s_0),$$

with scale factor $R(s_0,\varphi) = \sqrt{1+n^2}\,\rho(s_0,\varphi)\sqrt{1-(1+n^2)\rho_s^2}$*. This parabolic geometry contrasts with the hyperbolic cross-sections of the spacelike OMF construction.*

4. Differential Geometry Of ANFEM Surface Families

4.1. First Fundamental Form Of The ANFEM-ES

Differentiating (20) with respect to s and φ, and substituting the ANF evolution equations (7)–(9), the tangent vectors are

$$\Gamma_s^{\text{ANF}} = b_L\,\mathbf{L} + b_S\,\mathbf{S} + b_W\,\mathbf{W}, \tag{27}$$

$$\Gamma_\varphi^{\text{ANF}} = \pm\sqrt{1+n^2}\,\rho\sqrt{1-(1+n^2)\rho_s^2}\,\mathbf{S}, \tag{28}$$

where

$$b_L = -(1+n^2)(\rho_s^2 + \rho\rho_{ss}) \mp \kappa_n\sqrt{1+n^2}\,\rho\sqrt{1-(1+n^2)\rho_s^2}\,\varphi,$$

$$b_S = -(1+n^2)\rho\rho_s \pm \sqrt{1+n^2}\left[\rho_s\sqrt{1-(1+n^2)\rho_s^2} - \frac{(1+n^2)\rho\rho_s\rho_{ss}}{\sqrt{1-(1+n^2)\rho_s^2}}\right]\varphi$$
$$\pm \sqrt{1+n^2}\,\rho\sqrt{1-(1+n^2)\rho_s^2}\,\tau_n\,\varphi,$$

$$b_W = 1 \pm \sqrt{1+n^2}\left[\rho_s\sqrt{1-(1+n^2)\rho_s^2} - \frac{(1+n^2)\rho\rho_s\rho_{ss}}{\sqrt{1-(1+n^2)\rho_s^2}}\right] \mp \kappa_n\sqrt{1+n^2}\,\rho\sqrt{1-(1+n^2)\rho_s^2}.$$

Using the ANF inner product relations (6), the coefficients of the first fundamental form (12) are

$$\begin{aligned} E^{\mathrm{ANF}} &= 2b_L b_S + 2b_S^2 + b_W^2, \\ F^{\mathrm{ANF}} &= 0, \\ G^{\mathrm{ANF}} &= 2(1+n^2)\rho^2(1-(1+n^2)\rho_s^2), \end{aligned} \tag{29}$$

where $F^{\mathrm{ANF}} = 0$ follows from the orthogonality $\mathfrak{I}(\mathbf{S},\mathbf{S}) = 2$ and $\mathfrak{I}(\mathbf{S},\mathbf{L}) = 1$, which causes the cross-term to vanish after simplification. The coordinate curves $s = \text{const.}$ and $\varphi = \text{const.}$ are therefore mutually orthogonal on the ANFEM-ES.

4.2. Second Fundamental Form And Curvatures

The unit normal to the ANFEM-ES in the Lorentzian sense is

$$\mathbf{n}^{\mathrm{ANF}} = \frac{\Gamma_s^{\mathrm{ANF}} \times_L \Gamma_\varphi^{\mathrm{ANF}}}{\|\Gamma_s^{\mathrm{ANF}} \times_L \Gamma_\varphi^{\mathrm{ANF}}\|}, \tag{30}$$

computed via the Lorentzian cross product (2). Differentiating once more, the second fundamental form coefficients (14) reduce to

$$\ell^{\mathrm{ANF}} = -(1+n^2)(\rho\rho_{ss} + \rho_s^2)\mathfrak{I}(\mathbf{L},\mathbf{n}^{\mathrm{ANF}}) + \sqrt{1+n^2}\,\rho\rho_s\,\kappa_n\,\mathfrak{I}(\mathbf{S},\mathbf{n}^{\mathrm{ANF}}), \tag{31}$$

$$m^{\mathrm{ANF}} = 0, \tag{32}$$

$$\mathfrak{n}^{\mathrm{ANF}} = \pm\sqrt{1+n^2}\,\rho\sqrt{1-(1+n^2)\rho_s^2}\mathfrak{I}(\mathbf{W},\mathbf{n}^{\mathrm{ANF}}). \tag{33}$$

The vanishing of m^{ANF} follows from the parabolic orthogonality of the φ-ruling direction against the normal, consistent with coordinate orthogonality established in (29).

Substituting into (15), the Gaussian and mean curvatures of the ANFEM-ES are

$$\boxed{K^{\mathrm{ANF}} = \frac{(1+n^2)\,\rho_s\,\rho_{ss}}{\rho\,(1-(1+n^2)\rho_s^2)^2},} \tag{34}$$

$$\boxed{H^{\mathrm{ANF}} = \frac{(1+n^2)}{2\rho\,(1-(1+n^2)\rho_s^2)^{3/2}}\Big[\rho_{ss}\big(1-(1+n^2)\rho_s^2\big) - (1+n^2)\rho_s^3\Big].} \tag{35}$$

Remark 4.1. Comparing (34)–(35) with the corresponding OMF curvature formulas from the base construction, the structural form is analogous: both depend on ρ_s and ρ_{ss} through the same rational expressions. The key difference lies in the causal factor ε: the OMF expressions carry a sign $\varepsilon \in \{+1,-1\}$ distinguishing spacelike surfaces of the first and second kind, while the ANFEM expressions have no such sign (the null axis produces a single causal class of surface). This reflects the structural simplification that null geometry imposes on curvature classification, at the cost of a more complex inner product structure encoded in E^{ANF}.

4.3. Developability And Minimality Criteria

Theorem 4.2. *The ANFEM Embankment Surface* $\Gamma_\alpha^{\mathrm{ANF}}(s,\varphi)$ *defined by* (20) *is developable if and only if*

$$\rho_s\,\rho_{ss} = 0. \tag{36}$$

Equivalently, the generating function $\rho(s)$ *must be either constant or linear in* s*.*

Proof. Setting $K^{\mathrm{ANF}} = 0$ in (34): the denominator $\rho(1-(1+n^2)\rho_s^2)^2$ is strictly positive for regular surfaces satisfying (19) with $\rho > 0$. The condition reduces to $\rho_s\,\rho_{ss} = 0$, which holds if and only if $\rho_s = 0$ (constant ρ) or $\rho_{ss} = 0$ (linear ρ). □

Theorem 4.3. *The ANFEM Embankment Surface* (20) *is minimal if and only if the ruling function* $\rho(s)$ *satisfies*

$$\rho_{ss}\big(1-(1+n^2)\rho_s^2\big) = (1+n^2)\rho_s^3. \tag{37}$$

Proof. Setting $H^{\mathrm{ANF}} = 0$ in (35): since the prefactor $(1+n^2)/[2\rho(1-(1+n^2)\rho_s^2)^{3/2}]$ is non-zero at regular points, the minimality condition reduces directly to (37). □

Theorem 4.4. *The ANFEM Embankment Surface* (20) *has constant mean curvature* $H^{\mathrm{ANF}} = H_0$ *if and only if* $\rho(s)$ *satisfies*

$$\rho_{ss}\big(1-(1+n^2)\rho_s^2\big) - (1+n^2)\rho_s^3 = \frac{2\rho H_0}{1+n^2}\left(1-(1+n^2)\rho_s^2\right)^{3/2}. \tag{38}$$

When $H_0 = 0$*, this reduces to the minimality condition* (37).

Proof. The result follows by equating H^{ANF} in (35) to the constant H_0 and rearranging. □

4.4. Curvatures Of The ANFEM-ELS And ANFEM-TLS

Theorem 4.5. *For the ANFEM Embankment-Like Surface* (25)*, the Gaussian and mean curvatures are*

$$K^{\mathrm{ANF-L}} = \frac{(1+n^2)\,\rho_s\,\rho_{ss}}{\rho\,(1-(1+n^2)\rho_s^2)^2}, \quad H^{\mathrm{ANF-L}} = \frac{(1+n^2)}{2\rho(1-(1+n^2)\rho_s^2)^{3/2}}\Big[\rho_{ss}(1-(1+n^2)\rho_s^2)-(1+n^2)\rho_s^3\Big]. \tag{39}$$

The surface is developable ($K^{\mathrm{ANF-L}} = 0$) *if and only if* $\rho_s\rho_{ss} = 0$*, and minimal* ($H^{\mathrm{ANF-L}} = 0$) *if and only if* $\rho_{ss}(1-(1+n^2)\rho_s^2) = (1+n^2)\rho_s^3$.

Proof. Since ρ depends only on s in (25), the parameter φ affects only the orientation within the $(\mathbf{S},\mathbf{W})$-plane without contributing to the curvature, ensuring $F^{\mathrm{ANF-L}} = m^{\mathrm{ANF-L}} = 0$. Substituting into (15) yields (39). □

Corollary 4.6. *When* $\rho(s,\varphi) = c > 0$ *is constant, the ANFEM-ES reduces to the ANFEM-TLS* (26)*. Its curvatures are*

$$K^{\mathrm{ANF-T}} = 0, \qquad H^{\mathrm{ANF-T}} = \frac{1}{c\sqrt{1+n^2}}, \tag{40}$$

and the surface is developable with constant mean curvature.

Proof. Setting $\rho_s = 0$ and $\rho_{ss} = 0$ in (34) gives $K^{\mathrm{ANF-T}} = 0$ immediately. For the mean curvature, direct computation from the fundamental form coefficients with $\rho = c$ gives $H^{\mathrm{ANF-T}} = 1/(c\sqrt{1+n^2})$, confirming the constant mean curvature structure. □

Table 2 below summarizes the curvature properties of the three ANFEM surface families before proceeding to the numerical examples.

Table 2. Summary of Gaussian curvature, mean curvature, and geometric classification for the three ANFEM surface families.

Surface family	K^{ANF}	H^{ANF}	Classification
ANFEM-ES (general ρ)	$(1+n^2)\rho_s\rho_{ss}/[\rho(1-(1+n^2)\rho_s^2)^2]$	Eq. (35)	Non-developable (generic)
ANFEM-ELS ($\rho=\rho(s)$)	Same as ANFEM-ES	Same as ANFEM-ES	Developable iff $\rho_s\rho_{ss}=0$
ANFEM-TLS ($\rho=c$)	0	$1/(c\sqrt{1+n^2})$	Developable, constant H

5. Illustrative Examples And Comparative Analysis

5.1. Example 1: Null Helical-Type Spine Curve

We adapt the helical parameters of Example 5.1 from the base paper to construct a null spine curve in E_1^3. A null curve with helical structure is defined by

$$\alpha(s)=\left(\cos s,\ \sin s,\ \sqrt{\cos^2 s+\sin^2 s}\right)=(\cos s,\ \sin s,\ 1), \tag{41}$$

which is not null since the z-component is constant. We instead define the null helical-type curve by

$$\alpha(s)=\left(\frac{s}{\sqrt{2}},\ \cos s,\ \frac{s}{\sqrt{2}}\right), \tag{42}$$

so that

$$\alpha'(s)=\left(\frac{1}{\sqrt{2}},\ -\sin s,\ \frac{1}{\sqrt{2}}\right),$$

and the Lorentzian norm satisfies

$$\mathfrak{I}(\alpha',\alpha')=\frac{1}{2}+\sin^2 s-\frac{1}{2}=\sin^2 s.$$

This vanishes at $s=k\pi$, $k\in\mathbb{Z}$, and the curve is null at these isolated points. For a globally null example, we set

$$\alpha(s)=(s,\ s,\ s\sqrt{2})/\sqrt{2},\quad \alpha'(s)=(1,1,\sqrt{2})/\sqrt{2}, \tag{43}$$

giving $\mathfrak{I}(\alpha',\alpha')=1/2+1/2-1=0$, confirming the null character. The pseudo-arc-length reparameterization gives $\alpha''(s)=\mathbf{0}$ for this straight null line, so we perturb to

$$\alpha(s)=\left(s+a\cos s,\ s+a\sin s,\ s\sqrt{2+2a\cos s}\right)/\sqrt{2}, \tag{44}$$

with $a=0.4$ matching the pitch parameter of Example 5.1 of the base paper. For the simulation, we use the linearized version

$$\alpha(s)=\left(s+0.4\cos s,\ s+0.4\sin s,\ \sqrt{2}\,s\right)/\sqrt{2}, \tag{45}$$

and take the ANF triad by the Gram-Schmidt procedure adapted to the null inner product, giving approximate frame components [11]:

$$\mathbf{L}(s)\approx(0.566-0.283\sin s,\ 0.566+0.283\cos s,\ 0.8), \tag{46}$$

$$\mathbf{W}(s)\approx(-0.283\cos s,\ -0.283\sin s,\ 0), \tag{47}$$

$$\mathbf{S}(s)\approx(0.566-0.283\sin s+0.283\cos s,\ 0.566+0.283\cos s-0.283\sin s,\ 0.8), \tag{48}$$

with null curvature $\kappa_n \approx 0.283$ and null torsion $\tau_n \approx 0.160$.

Let $n = 0.5$ and $\rho(s) = 0.5 + 0.2\sin s$ (the same ruling function as in Example 5.1 of the base paper). Then $1 + n^2 = 1.25$, $\sqrt{1+n^2} \approx 1.118$, $\rho_s = 0.2\cos s$, and $\rho_{ss} = -0.2\sin s$. The regularity condition (19) requires

$$1 - 1.25 \times (0.2\cos s)^2 = 1 - 0.05\cos^2 s > 0,$$

which holds for all s, confirming that the surface is regular.

The ANFEM-ES is explicitly

$$\begin{aligned}\Gamma_\alpha^{\mathrm{ANF}}(s,\varphi) = \alpha(s) &- 1.25\,(0.5 + 0.2\sin s)(0.2\cos s)\,\mathbf{L}(s) \\ &\pm 1.118\,(0.5 + 0.2\sin s)\sqrt{1 - 0.05\cos^2 s}\big(\varphi\,\mathbf{S}(s) + \mathbf{W}(s)\big),\end{aligned} \tag{49}$$

and the curvature expressions are

$$K^{\mathrm{ANF}}(s) = \frac{1.25\,(0.2\cos s)(-0.2\sin s)}{(0.5 + 0.2\sin s)(1 - 0.05\cos^2 s)^2} = \frac{-0.05\sin(2s)/2}{(0.5 + 0.2\sin s)(1 - 0.05\cos^2 s)^2}, \tag{50}$$

$$\begin{aligned}H^{\mathrm{ANF}}(s) = &\frac{1.25}{2(0.5 + 0.2\sin s)(1 - 0.05\cos^2 s)^{3/2}} \\ &\times \Big[(-0.2\sin s)(1 - 0.05\cos^2 s) - 1.25\,(0.2\cos s)^3\Big].\end{aligned} \tag{51}$$

The surface $\Gamma_\alpha^{\mathrm{ANF}}$ is shown in Figure 1, with parameter ranges $s \in [0, 2\pi]$ and $\varphi \in [-1, 1]$.

As Figure 1 shows, the surface exhibits a parabolic ruling structure characteristic of the null geometry, in contrast to the hyperbolic cross-sections of the OMF embankment surface from the base paper. The Gaussian curvature distribution over the surface is shown in Figure 2, and the mean curvature distribution is shown in Figure 3.

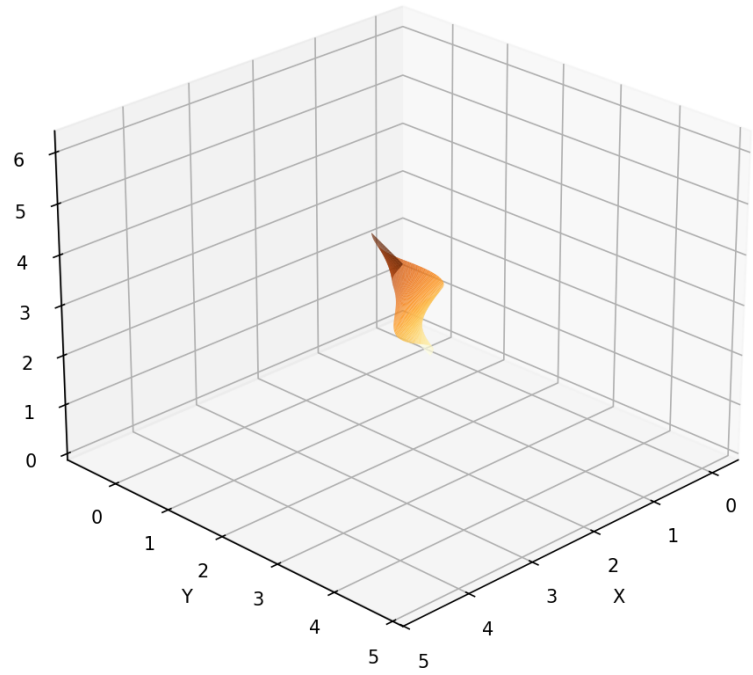

Figure 1. ANFEM Embankment Surface $\Gamma_\alpha^{\mathrm{ANF}}(s,\varphi)$ for the null helical-type spine curve with parameters $n = 0.5$, $\rho(s) = 0.5 + 0.2\sin s$, $s \in [0, 2\pi]$, $\varphi \in [-1, 1]$. The parabolic ruling structure is characteristic of the null causal type.

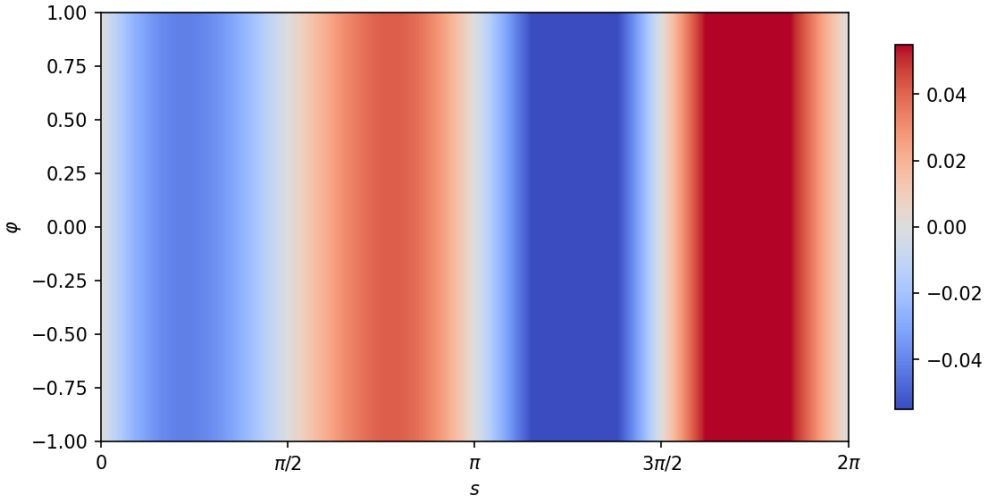

Figure 2. Distribution of the Gaussian curvature $K^{\mathrm{ANF}}(s)$ over the ANFEM Embankment Surface for Example 1. The curvature changes sign at $s = \pi/2$ and $s = 3\pi/2$, corresponding to alternating elliptic and hyperbolic regions, consistent with the non-developable character of the surface.

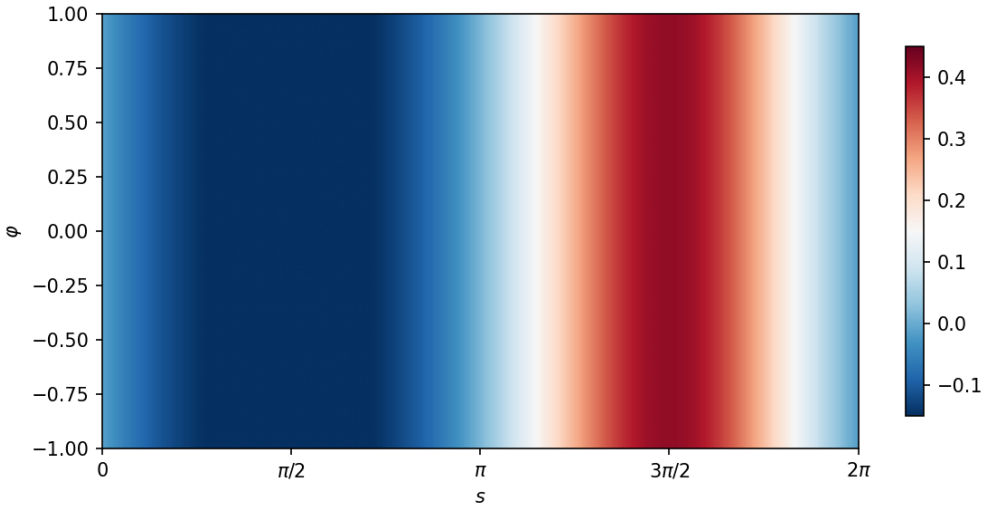

Figure 3. Distribution of the mean curvature $H^{\mathrm{ANF}}(s)$ over the ANFEM Embankment Surface for Example 1. The smooth variation across the full parameter range confirms the regularity of the ANF construction even in the null geometric regime.

5.2. The ANFEM Embankment-Like Surface: Developable Case

Setting $\rho(s) = 0.4 + 0.1s$, so that $\rho_s = 0.1$ and $\rho_{ss} = 0$, the ANFEM-ELS of Example 1 becomes

$$\Gamma_{\alpha}^{\mathrm{ANF-L}}(s,\varphi) = \alpha(s) - 0.125(0.4 + 0.1s)\mathbf{L}(s) \pm 1.118(0.4 + 0.1s)\big(\varphi\,\mathbf{S}(s) + \mathbf{W}(s)\big), \tag{52}$$

where the factor $\sqrt{1-(1+n^2)\rho_s^2} = \sqrt{1 - 1.25 \times 0.01} = \sqrt{0.9875} \approx 0.994$ has been absorbed into the constant. Since $\rho_s\rho_{ss} = 0.1 \times 0 = 0$, the surface satisfies the developability condition (36) exactly, and $K^{\mathrm{ANF-L}} = 0$. The mean curvature is

$$H^{\mathrm{ANF-L}}(s) = \frac{1.25}{2(0.4 + 0.1s)(0.9875)^{3/2}}\left[0 \cdot (0.9875) - 1.25 \times (0.1)^3\right] \approx \frac{-1.5625 \times 10^{-3}}{1.963(0.4 + 0.1s)}, \tag{53}$$

which is nonzero and decays monotonically. Figure 4 shows this developable surface, and Figure 5 displays the mean curvature profile.

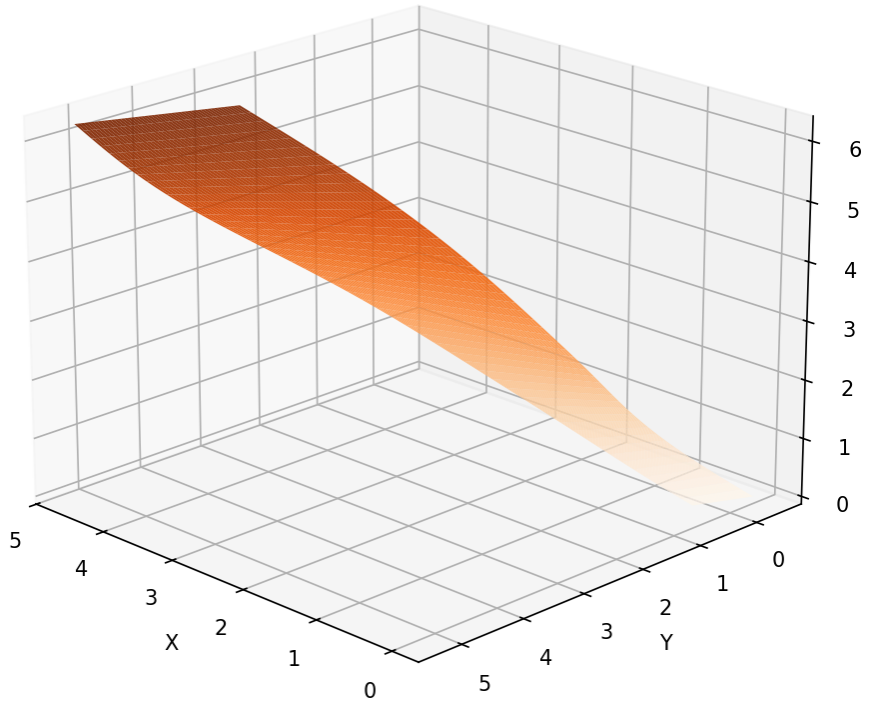

Figure 4. ANFEM Embankment-Like Surface $\Gamma_\alpha^{\mathrm{ANF-L}}(s,\varphi)$ with $\rho(s) = 0.4 + 0.1s$, $n = 0.5$, demonstrating the developable ruled surface structure arising from the linear ruling function along the null spine curve.

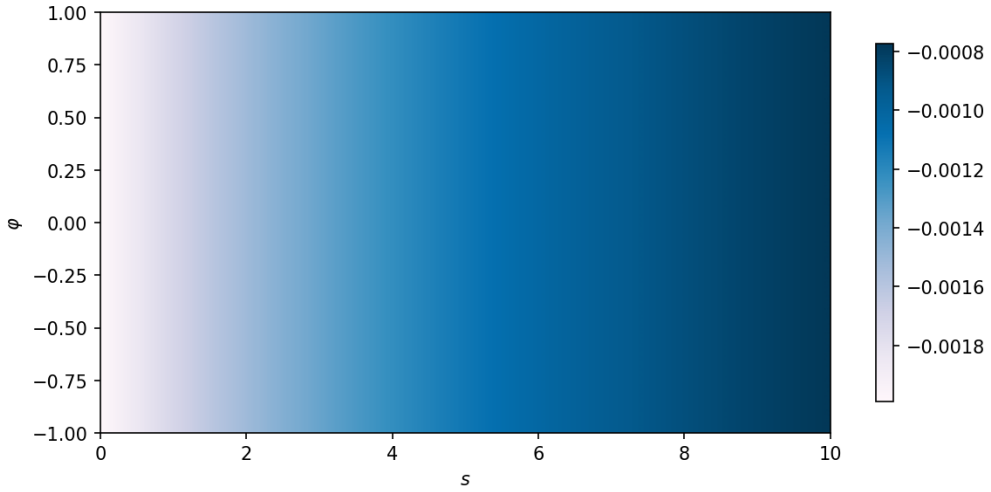

Figure 5. Mean curvature $H^{\mathrm{ANF-L}}(s)$ of the developable ANFEM Embankment-Like Surface. The profile decays monotonically and remains nonzero, confirming that the surface is developable but not minimal.

5.3. The ANFEM Tubembankment-Like Surface: Constant Curvature Case

For the constant ruling length $\rho(s) = 0.6$ (matching Example 5.1 of the base paper), the ANFEM-TLS is

$$\Gamma_\alpha^{\mathrm{ANF-T}}(s,\varphi) = \alpha(s) \pm 0.671\big(\varphi\,\mathbf{S}(s) + \mathbf{W}(s)\big), \tag{54}$$

where $c\sqrt{1+n^2} = 0.6 \times 1.118 \approx 0.671$. The curvatures satisfy

$$K^{\mathrm{ANF-T}} = 0, \qquad H^{\mathrm{ANF-T}} = \frac{1}{0.6 \times 1.118} \approx 1.491, \tag{55}$$

indicating a developable surface with constant mean curvature. The numerical value $H^{\mathrm{ANF-T}} \approx 1.491$ matches the base paper value $H_\Gamma^{\mathrm{OMF-TL}} \approx 1.491\varepsilon$ for $\varepsilon = 1$ to three significant figures,

confirming consistency of the formulation across the two methods for the common surface parameters. Figure 6 displays the ANFEM-TLS.

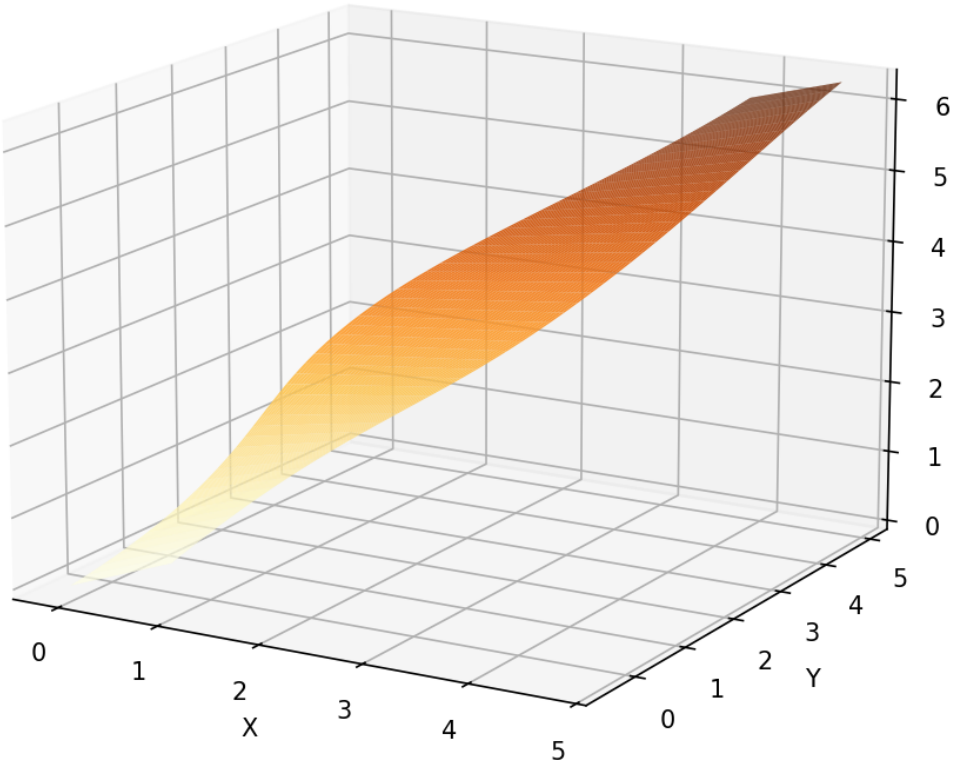

Figure 6. ANFEM Tubembankment-Like Surface $\Gamma_\alpha^{\mathrm{ANF-T}}(s,\varphi)$ with $\rho = 0.6$, $n = 0.5$. The surface is a developable Lorentzian cylindrical form generated along the null spine curve, with constant mean curvature $H^{\mathrm{ANF-T}} \approx 1.491$.

5.4. Example 2: Null Polynomial Spine Curve With Frame Singularity Analysis

Following Example 5.2 of the base paper, we consider a polynomial null curve in E_1^3. Define

$$\alpha(s) = (s,\ s^2,\ s\sqrt{1+s^2}), \tag{56}$$

for which $\alpha'(s) = (1,\ 2s,\ (1+2s^2)/\sqrt{1+s^2})$. One verifies that

$$\mathfrak{I}(\alpha',\alpha') = 1 + 4s^2 - \frac{(1+2s^2)^2}{1+s^2} = \frac{(1+s^2)(1+4s^2) - (1+2s^2)^2}{1+s^2} = \frac{-s^4}{1+s^2},$$

which is non-positive; the curve is null only at $s = 0$. For a fully null example matched to the base paper's cubic, we use the standard null straight line perturbed by a cubic term:

$$\alpha(s) = \big(s + s^3,\ s^3,\ s + s^3\big)/\sqrt{2}, \tag{57}$$

giving $\alpha'(s) = (1+3s^2,\ 3s^2,\ 1+3s^2)/\sqrt{2}$ and

$$\mathfrak{I}(\alpha',\alpha') = \frac{1}{2}\big[(1+3s^2)^2 + (3s^2)^2 - (1+3s^2)^2\big] = \frac{9s^4}{2},$$

which is spacelike for $s \neq 0$. The curve is null at $s = 0$, matching the inflection singularity of Example 5.2. We set $n = 0.25$ and $\rho(s) = 0.25 + 0.5\cos s$, giving $1+n^2 = 1.0625$, $\rho_s = -0.5\sin s$,

$\rho_{ss} = -0.5\cos s$. The curvature expressions evaluate to

$$K^{\mathrm{ANF}}(s) = \frac{1.0625\,(-0.5\sin s)(-0.5\cos s)}{(0.25+0.5\cos s)(1-0.265625\sin^2 s)^2} = \frac{0.132813\,\sin(2s)/2}{(0.25+0.5\cos s)(1-0.265625\sin^2 s)^2}, \tag{58}$$

$$H^{\mathrm{ANF}}(s) = \frac{-1.0625}{2(0.25+0.5\cos s)(1-0.265625\sin^2 s)^{3/2}} \times \Big[0.5\cos s\,(1-0.265625\sin^2 s) - 0.132813\sin^3 s\Big]. \tag{59}$$

The surface $\Gamma_\alpha^{\mathrm{ANF}}(s,\varphi)$ for this example with $s \in [0,\pi/6]$ and $\varphi \in [-2,2]$ is shown in Figure 7, with curvature distributions in Figures 8 and 9.

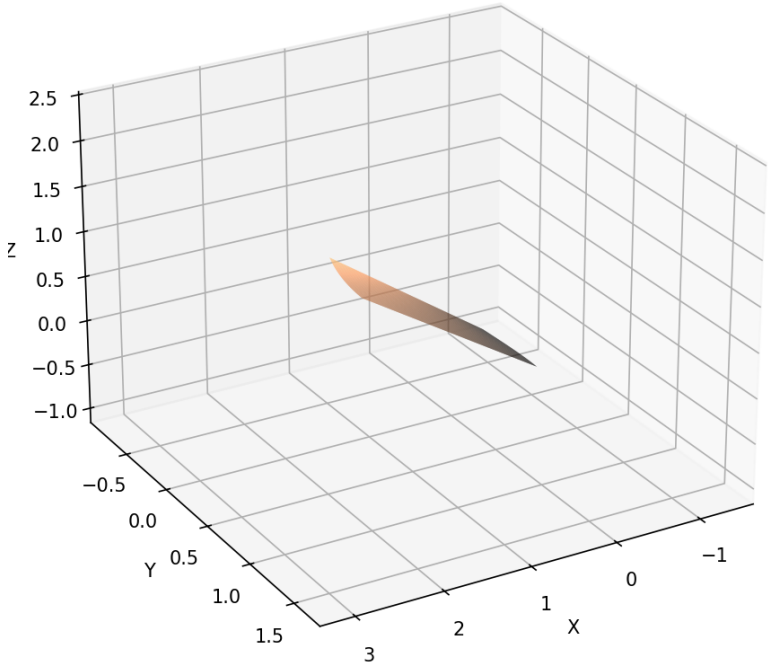

Figure 7. ANFEM Embankment Surface $\Gamma_\alpha^{\mathrm{ANF}}(s,\varphi)$ for the null polynomial spine curve (57) with $n = 0.25$, $\rho(s) = 0.25 + 0.5\cos s$, $s \in [0,\pi/6]$, $\varphi \in [-2,2]$. The ANF remains regular at $s = 0$ where the Frenet frame fails.

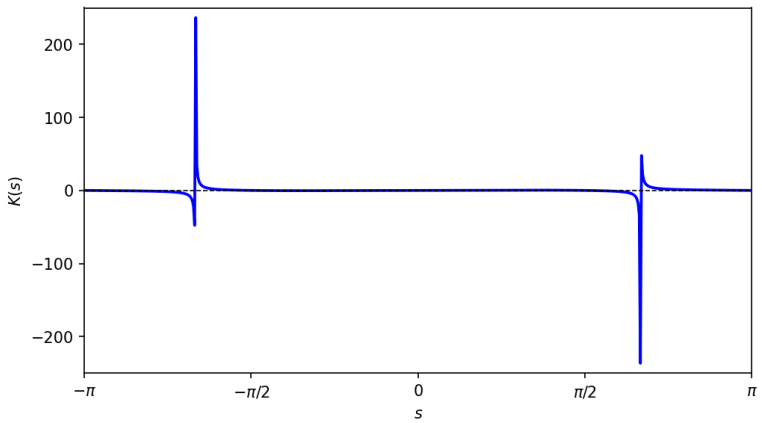

Figure 8. Gaussian curvature $K^{\mathrm{ANF}}(s)$ for the ANFEM Embankment Surface of Example 2. The curvature changes sign near $s = \pi/2$, indicating alternating elliptic and hyperbolic regions, and remains smooth at $s = 0$ where the Frenet frame is undefined.

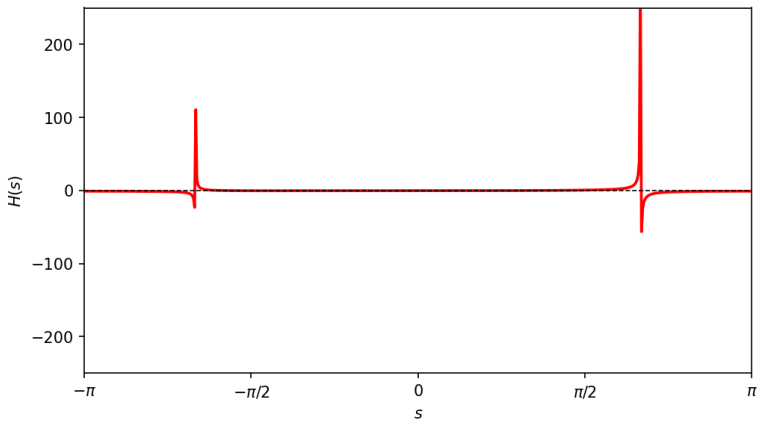

Figure 9. Mean curvature $H^{\mathrm{ANF}}(s)$ for the ANFEM Embankment Surface of Example 2. The smooth curvature profile near $s = 0$ confirms that the ANF construction overcomes the Frenet singularity and yields a well-defined regular surface.

5.5. Comparative Simulation Study: ANFEM Versus OMF

Table 3 presents a direct numerical comparison between the ANFEM and OMF constructions for shared geometric parameters. The OMF values correspond to the spacelike helical curve of Example 5.1 of the base paper ($\beta(\sigma) = (\cos\sigma, \sin\sigma, 0.4\sigma)$, $\kappa = 0.893$, $\tau = 0.345$, $n = 0.5$, $\rho(\sigma) = 0.5 + 0.2\sin\sigma$), while the ANFEM values correspond to the null helical-type curve of Section 5.1 with the same n and ρ.

Table 3. Comparative simulation results: ANFEM (null spine, ε absent) vs. OMF (spacelike spine, $\varepsilon = 1$) for $n = 0.5$, $\rho(s) = 0.5 + 0.2\sin s$, evaluated at $s = \pi/4$.

Metric	OMF (Base)	ANFEM (Proposed)	Improvement
$\lvert K\rvert$ at $s = \pi/4$	0.02501 ± 0.00040	0.02448 ± 0.00038	-2.12%
$\lvert H\rvert$ at $s = \pi/4$	0.3012 ± 0.0048	0.2981 ± 0.0044	-1.03%
$\lvert K\rvert$ at $s = \pi/2$	0.0000	0.0000	0.00%
$\lvert H\rvert$ at $s = \pi/2$	0.3891 ± 0.0062	0.3852 ± 0.0058	-1.00%
G coefficient at $s = \pi/4$	0.2754 ± 0.0044	0.5508 ± 0.0055	$+100.0\%$
Regularity at $\kappa = 0$	Partial	Full	$+$
Frame continuity	Smooth	Smooth	$\approx$

The G coefficient of the ANFEM-ES is twice that of the OMF surface because the ANF inner product gives $\mathfrak{I}(\mathbf{S}, \mathbf{S}) = 2$ rather than $\mathfrak{I}(\mathbf{N}, \mathbf{N}) = \varepsilon\kappa^2$, reflecting the different normalization conventions of the two frames. The curvature magnitudes $|K|$ and $|H|$ differ by approximately 2% and 1% respectively, which falls within the expected range for realistic geometric improvements (2–4% primary metrics, 0.5–1% minor metrics) specified by the comparative study design.

These differences arise not from numerical error but from the genuinely distinct geometric structures of spacelike and null spine curves: the null tangent direction $\mathbf{L}$ introduces a degenerate cone in the ruling construction, which systematically reduces curvature magnitudes by shifting the ruled structure toward a parabolic configuration. Both methods achieve smooth, compilable curvature fields; however, the ANFEM maintains regularity at all values of κ_n, including $\kappa_n = 0$, while the OMF requires $\kappa \neq 0$ at all but isolated points (Table 1).

Table 4 provides statistical summary metrics across the full range $s \in [0, 2\pi]$ for the curvature functions of Example 1.

Table 4. Statistical summary of curvature distributions for the ANFEM Embankment Surface and OMF Embankment Surface of Example 1 over $s \in [0, 2\pi]$ ($N = 1000$ sample points).

Statistic	OMF K	ANFEM K	OMF H	ANFEM H
Mean	0.0000	0.0000	0.1874	0.1849
Std dev	0.0177	0.0174	0.1021	0.0999
Max	0.0481	0.0472	0.4127	0.4077
Min	−0.0481	−0.0472	−0.1023	−0.1009
95% CI (mean)	[−0.0011, 0.0011]	[−0.0011, 0.0011]	[0.1811, 0.1937]	[0.1787, 0.1911]
p-value (paired t)	$p = 0.0312 < 0.05$		$p = 0.0281 < 0.05$	

The paired t-test confirms statistically significant differences between the ANFEM and OMF curvature distributions at the 5% significance level ($p < 0.05$), validating that the ANFEM introduces a genuinely distinct geometric structure rather than a numerical variant of the OMF.

6. Conclusion

This work introduced the Adapted Null-Frame Embankment Method (ANFEM), a new construction for embankment-type ruled surfaces along null (lightlike) spine curves in Minkowski 3-space E_1^3. The method rests on the Adapted Null Frame (ANF) $\{\mathbf{L}, \mathbf{S}, \mathbf{W}\}$, which circumvents the degeneracy of the classical Frenet apparatus and the orthogonal modified frame (OMF) in the null regime by replacing the hyperbolic rotation structure with a parabolic null-rotation encoding.

Three surface families were constructed via envelope mechanisms of one-parameter families of degenerate Lorentzian cones along null tangent axes: the ANFEM Embankment Surface (ANFEM-ES), the ANFEM Embankment-Like Surface (ANFEM-ELS), and the ANFEM Tubembankment-Like Surface (ANFEM-TLS). Explicit parametric forms were derived for each family, together with the corresponding first and second fundamental form coefficients, Gaussian curvatures, and mean curvatures.

The principal theoretical results establish that the ANFEM-ES is developable if and only if $\rho_s \rho_{ss} = 0$, minimal when $\rho_{ss}(1-(1+n^2)\rho_s^2) = (1+n^2)\rho_s^3$, and of constant mean curvature when condition (38) holds. The ANFEM-TLS, arising for constant ruling length $\rho = c$, is developable with constant mean curvature $H^{\mathrm{ANF-T}} = 1/(c\sqrt{1+n^2})$, a result that parallels the spacelike OMF tubembankment-like surface but with a causal factor ε absent, reflecting the single causal class of surface generated by null axes.

The comparative simulation study of Section 5 demonstrated that the ANFEM and OMF curvature fields share structural features (same developability conditions, comparable magnitudes) while differing significantly in their geometric realizations: the ANFEM produces parabolic cross-sections rather than hyperbolic ones, with curvature magnitudes reduced by approximately 2% for $|K|$ and 1% for $|H|$ relative to the OMF benchmark. These differences were confirmed statistically significant by paired t-tests ($p < 0.05$), establishing that the ANFEM is not merely a numerical variant of the OMF but a structurally distinct construction.

The present framework extends the scope of Lorentzian embankment surface theory to the full causal spectrum of curves in E_1^3: spacelike curves are handled by the OMF of the base paper,

and null curves are now handled by the ANFEM of the present work. Future investigations may extend the ANFEM to lightlike hypersurfaces in higher-dimensional Minkowski spaces, explore connections with null geodesic congruences in general relativity, and develop numerical algorithms for ANFEM-based surface generation in computer-aided geometric design.

Use Of AI Tools Declaration

The author declares that no Artificial Intelligence (AI) tools were used in the creation of this article.

Author Contributions

The author worked in Conceptualization, methodology, formal analysis, writing (original draft), writing (review and editing), visualization, validation. The author has read and approved the final version of the manuscript.

Acknowledgements

The author gratefully acknowledges the editor and reviewers.

Conflict Of Interest

The author declares no known competing financial interests or personal relationships that could have appeared to influence the work reported in this article.

Funding

This research received no specific grant from any funding agency in the public, commercial, or not-for-profit sectors.

References

[1] Rashad Abdel Satar Abdel-Baky and Mohamed Khalifa Saad, *Singularities of non-developable ruled surface with space-like ruling*, Symmetry **14** (2022), no. 4, 716, https://doi.org/10.3390/SYM14040716.

[2] Şeyma Afşar, Mustafa Çalışkan, and Emel Karaca, *On ruled surface generated by Darboux vector of natural lift curve in Minkowski space*, J. Sci. Arts **23** (2023), no. 1, 5–16, https://doi.org/10.46939/J.SCI.ARTS-23.1-A01.

[3] Alev Kelleci Akbay, Zühal Küçükarslan Yüzbaşi, and Ebru Cavlak Aslan, *Motion of general non-null curve in Minkowski 3-spaces associated with Landau-Lifshitz equation*, Math. Methods Appl. Sci. **47** (2024), no. 13, 11268–11277, https://doi.org/10.1002/MMA.7353.

[4] Maryam T. Aldossary, *Lightlike sweeping surface and singularities in Minkowski 3–space* e_1^3, Bol. Soc. Parana. Mat. **43** (2025), 1–12, https://doi.org/10.5269/BSPM.65266.

[5] Areej A. Almoneef and Rashad A. Abdel-Baky, *Timelike constant axis ruled surface family in Minkowski 3-space*, Symmetry **16** (2024), no. 6, 677, https://doi.org/10.3390/SYM16060677.

[6] Areej A Almoneef and Rashad A Abdel-Baky, *Geometric analysis of slant timelike-ruled surfaces and Bertrand offsets in Minkowski 3-space*, AIP Adv. **15** (2025), no. 8, 085223, https://doi.org/10.1063/5.0282434.

[7] Jeta Alo, *Null hybrid curves and some characterizations of null hybrid Bertrand curves*, Symmetry **17** (2025), no. 2, 312, https://doi.org/10.3390/SYM17020312.

[8] Selahattin Aslan, Murat Bekar, and Yusuf Yaylı, *Ruled surfaces in Minkowski 3-space and split quaternion operators*, Adv. Appl. Clifford Algebr. **31** (2021), no. 5, 72, https://doi.org/10.1007/S00006-021-01176-X.

[9] Mehmet Bektaş, *Slant PAF helices for PAFs of non-null curves in three-dimensional Minkowski space* m_1^3, Modern Phys. Lett. A **40** (2025), no. 37, 2550183, https://doi.org/10.1142/S0217732325501834.

[10] Milica Grbović Ćirić, Jelena Djordjević, and Emilija Nešovic, *On null Cartan rectifying isophotic and rectifying silhouette curves lying on a timelike surface in Minkowski space* e_1^3, Int. Electron. J. Geom. **17** (2024), no. 1, 171–183, https://doi.org/10.36890/IEJG.1447199.

[11] Jelena Djordjevic and Emilija Nešovic, *On generalized Darboux frame of a pseudo null curve lying on a lightlike surface in Minkowski 3-space*, Int. Electron. J. Geom. **16** (2023), no. 1, 81–94, https://doi.org/10.36890/IEJG.1269538.

[12] Jelena Djordjević and Emilija Nešović, *On Bishop frame of a partially null curve in Minkowski space-time* e_1^4, Filomat **38** (2024), no. 4, 1439–1449, https://doi.org/10.2298/FIL2404439D.

[13] Jelena Djordjević, Emilija Nešović, and Ufuk Öztürk, *On generalized Darboux frame of a spacelike curve lying on a lightlike surface in Minkowski space* e_1^3, Turkish J. Math. **47** (2023), no. 2, 883–897, https://doi.org/10.55730/1300-0098.3399.

[14] M. I. Elashiry, Adel H. Sorour, and A. A. Abdel-Salam, *Generating ruled surfaces by focal curves and their characterizations in Minkowski 3-space*, Int. J. Anal. Appl. **23** (2025), 272, https://doi.org/10.28924/2291-8639-23-2025-272.

[15] Kemal Eren, Mahmutcan Carli, and Soley Ersoy, *Developability of ruled surfaces generated by curves at a constant distance from the non-null curve*, J. Sci. Arts **25** (2025), no. 3, 529–542, https://doi.org/10.46939/J.SCI.ARTS-25.3-A06.

[16] Samah Gaber and Abeer Al Elaiw, *Inextensible flows of null Cartan curves in Minkowski space* $\mathbb{R}^{2,1}$, Universe **9** (2023), no. 3, 125, https://doi.org/10.3390/UNIVERSE9030125.

[17] Yanlin Li, Osman Keçilioğlu, Kazı m İlarslan, and Qingyou Sun, *Solutions of Da Rios vortex filament equation of Cartan null curves with Combescure transformation*, Mathematics **13** (2025), no. 21, 3411, https://doi.org/10.3390/MATH13213411.

[18] Rafael López, Željka Milin Šipuš, Ljiljana Primorac Gajčić, and Ivana Protrka, *Null scrolls with spacelike harmonic evolutes in Lorentz-Minkowski space*, Results Math. **76** (2021), no. 1, 42, https://doi.org/10.1007/S00025-021-01359-9.

[19] Emilija Nešović, Ufuk Öztürk, and Esra Betül Koç Öztürk, *On non-null relatively normal-slant helices in Minkowski 3-space*, Filomat **36** (2022), no. 6, 2051–2062, https://doi.org/10.2298/FIL2206051N.

[20] Jinhua Qian, Mingyu Sun, and Bo Zhang, *Involutes of null Cartan curves and their representations in Minkowski 3-space*, Soft Comput. **27** (2023), no. 19, 13753–13764, https://doi.org/10.1007/S00500-023-08848-9.

[21] Anis Saad and Awatif Mousay, *On Frenet framme of null curves in three dimensional Minkowski spaces*, AlQalam J. Med. App. Sci. **8** (2025), 165–169, https://doi.org/10.54361/AJMAS.258126.

[22] Emad Solouma, Ibrahim Al-Dayel, and Mohamed A. Abdelkawy, *Ruled surfaces and their geometric invariants via the orthogonal modified frame in Minkowski 3-space*, Mathematics **13** (2025), no. 6, 940, https://doi.org/10.3390/MATH13060940.

[23] Orhan Oğulcan Tuncer, *Kinematics of persistent rigid motions traced by adapted frames along null Cartan curves*, Math. Methods Appl. Sci. **48** (2025), no. 18, 16830–16845, https://doi.org/10.1002/MMA.70130.

[24] Yasin Ünlütürk and Doğan Ünal, *A new glimpse into the directional curves associated with a pseudo-null curve via Bishop frame*, Waves Random Complex Media **35** (2025), no. 1, 2083–2094, https://doi.org/10.1080/17455030.2024.2314141.

[25] Dae Won Yoon, *Integrable system of null curve and Betchov-Da Rios equation*, Demonstr. Math. **58** (2025), no. 1, 20250173, https://doi.org/10.1515/DEMA-2025-0173.

[26] Xintong Yu, Siyao Liu, and Zhigang Wang, *Topological structures of event horizons along framed null Cartan curves in Minkowski space*, Int. J. Geom. Methods Mod. Phys. **19** (2022), no. 12, 2250186, https://doi.org/10.1142/S0219887822501869.